Virologica Sinica (2021) 36:1554–1565
https://doi.org/10.1007/s12250-021-00445-0

www.virosin.org
www.springer.com/12250

RESEARCH ARTICLE

Integrated Metabolomics and Transcriptomics Analyses Reveal Metabolic Landscape in Neuronal Cells during JEV Infection

Mengyuan Li[1] · Jiali Yang[2] · Chuantao Ye[1] · Peiyu Bian[1] · Xiaofei Yang[1] · Haijun Zhang[3] · Chuanyu Luo[4] · Zhifeng Xue[4] · Yingfeng Lei[5] · Jianqi Lian[1]

Received: 25 April 2021 / Accepted: 9 August 2021 / Published online: 24 September 2021

Abstract

Japanese encephalitis virus (JEV) is a leading cause of viral encephalitis in endemic regions of Asia. The neurotropism of JEV and its high-efficiency replication in neurons are the key events for pathogenesis. Revealing the interplay between virus and host cells in metabolic facet is of great importance both for unraveling the pathogenesis mechanisms and providing novel antiviral targets. This study took advantage of the integration analysis of metabolomics and transcriptomics to depict the metabolic profiles of neurons during the early stage of JEV infection. Increased glycolysis and its branched pentose phosphate pathway (PPP) flux and impaired oxidative phosphorylation (OXPHOS) in glucose utilization, and the catabolic patterns of lipid metabolism were created to facilitate the biosynthesis of precursors needed for JEV replication in neurons. Pharmacological inhibitions of both glycolysis pathway and PPP in neurons suggested its indispensable role in maintaining the optimal propagation of JEV. In addition, analysis of metabolomic-transcriptomic regulatory network showed the pivotal biological function of lipid metabolism during JEV infection. Several pro-inflammatory lipid metabolites were significantly up-regulated and might partially be responsible for the progression of encephalitis. These unique metabolic reprogramming features might give deeper insight into JEV infected neurons and provide promising antiviral approaches targeting metabolism.

Keywords Japanese encephalitis virus (JEV) · Metabolomics · Transcriptomics · Metabolic reprogramming

Introduction

Japanese encephalitis (JE) is an acute inflammatory disease of the central nervous system caused by the Japanese encephalitis virus (JEV), a mosquito-borne flavivirus and a leading cause of epidemic encephalitis in Asia. JEV belongs to the genus *Flavivirus* of the *Flaviviridae* family, which includes West Nile virus (WNV), dengue virus (DENV), Zika virus (ZIKV), yellow fever virus (YFN) and tick-borne encephalitis virus (TBEV) (Barrows *et al.* 2018). As a neurotropic virus, JEV can effectively cross the blood-brain barrier (BBB) to induce acute viral encephalitis syndromes such as fever, coma, seizures, paralysis and even death in humans. While JEV causes high morbidity and mortality, there is no specific and effective therapy available for JE (Erlanger *et al.* 2009).

Since viruses are obligate intracellular parasites, it is no wonder that they rely on host cell machinery to complete their entire life cycle. Different viruses may adopt different strategies in rewiring host cellular metabolism (Thaker

Mengyuan Li and Jiali Yang have contributed equally to this work.

Supplementary Information The online version contains supplementary material available at https://doi.org/10.1007/s12250-021-00445-0.

✉ Jianqi Lian
lianjq@fmmu.edu.cn

✉ Yingfeng Lei
yflei@fmmu.edu.cn

[1] Department of Infectious Diseases, Tangdu Hospital, Air Force Medical University, Xi'an 710038, China

[2] Key Laboratory of Resource Biology and Biotechnology in Western China, Ministry of Education, College of Life Sciences, Northwest University, Xi'an 710069, China

[3] Department of Neurology, Xijing Hospital, Air Force Medical University, Xi'an 710032, China

[4] Pathogenic Biology, Medical College of Yan'an University, Yan'an 716000, China

[5] Department of Microbiology, School of Preclinical Medicine, Air Force Medical University, Xi'an 710032, China

et al. 2019b). However, anabolic phenotype conferred by virus infection is usually common and often similar to tumor cells, like up-regulated nutrients consumption, increased nucleotide and lipid biosynthesis in coping with the high viral needs for proliferative infection (Su *et al.* 2014; Warburg 1956). Changes take place in cell metabolic state further affect several cell physiological functions, such as cell division and apoptosis. Meanwhile, viruses also have developed multiple strategies to either stimulate or inhibit the metabolism to achieve its desired outcome. However, diverse viruses evolved distinct tactics to cope with different host cells and then lead to dissimilar metabolic landscapes (Mayer *et al.* 2019). Currently, whether or how JEV interacts with host cells in metabolic facet during infection is still unknown.

As is well-known, JEV is a typical neurotropic virus. Neurons are the dominant cells in brain favored by JEV infection and propagation. Here, we employed untargeted liquid chromatography-tandem mass spectrometry (LC-MS)-based metabolomics and Illumina sequencing platform-based transcriptomics to detect metabolites and genes in Neuro2a cells infected with JEV at 24 h post of infection (hpi). A large number of differential metabolites and genes were identified in JEV-infected Neuro2a cells compared to the mock-infected group. Increased glycolysis and its branched pentose phosphate pathway (PPP) flux and impaired oxidative phosphorylation (OXPHOS) in glucose utilization, accompanied with the catabolic pattern of lipid metabolism, were generated to facilitate the biosynthesis of precursors needed for viral replication. Pharmacological inhibitions of both glucose and lipid metabolism could effectively inhibit JEV replication either in Neuro2a cell line or mouse primary neurons. Our results indicated that JEV infection drastically reshaped the metabolic features in neurons to satisfy its own replication. Thus, metabolic facet may be a potential antiviral target in JEV infection.

Materials and Methods

Cells and Virus

The mouse neuroblastoma cell line Neuro2a and baby hamster kidney (BHK-21) cells were cultured in Dulbecco's modified Eagle's medium (DMEM, Corning, NY, USA) containing 10% fetal bovine serum (FBS, Gibco, Grand Island, NY, USA) and 1% penicillin/streptomycin (Hyclone, Logan, UT, USA). All cell lines were deposited and thawed in our laboratory. Primary mouse neurons were purchased from JingKang Bio (Shanghai, China). The propagation of JEV wild-type strain P3 in C6/36 cells was described as elsewhere (Bian *et al.* 2017).

Reagents

2-Dexoy-D-Glucose (2-DG), (L)-sodium lactate, 6-Aminonicotinamide (6-AN), ND-630, Etomoxir sodium salt, D-ribose 5-phosphate and Atglistatin (ATGL) were obtained from Topscience (Shanghai, China) and diluted in accordance with the instruction.

Cell Viability Assay

Neuro2a cells were seeded into 96-well plates at a density of 5×10^3/well and incubated with DMEM containing 2% FBS overnight. Cell culture medium then replaced with 2% FBS DMEM with different concentrations of inhibitors and incubated for 24 h. Then, 10 μL of Cell Counting Kit-8 (CCK-8, ThermoFisher, USA) solution were added to each well and incubated for 4 h. The absorbance of each well was measured at 450 nm using a microplate reader (Bio-Tek, USA). All experiments were performed in quintuplicate.

Viral Infection and Drugs Treatment

Neuro2a cells with 80% confluence were infected with mock (virus suspension inactivated by heat at 56 °C for 30 min) or JEV at MOI of 0.1 for 2 h in serum-free DMEM. Then, the inoculum was removed and cells were washed twice with PBS. Cells were subsequently incubated in fresh DMEM containing 2% FBS and 1% antibiotics alone or added with different inhibitors at 37 °C for 24 h. The steps of primary neurons infection were the same as Neuro2a cell line, but Neurobasal medium (Gibco, New York, USA) was especially used for primary neurons.

The protocol of ATGL pre-treatment is as follows. Neuro2a cells were pre-treated with ATGL for 12 h before infection, then the medium containing ATGL was removed and cells were washed twice with PBS. Infection of JEV was then performed and subsequently incubated in fresh DMEM containing 2% FBS and 1% antibiotics for 24 h.

Sample Collection for Metabolomic and Transcriptomic Analysis

1×10^7 Neuro2a cells were seeded in 15 cm cell culture dishes until completely adherent. After JEV- or mock-infected for 24 h, the supernatants were discarded and the cells were washed three times with PBS and scraped. Harvested cells were immediately snap-frozen in liquid nitrogen and stored at −80 °C for measurement.

Metabolites Extraction and LC-MS/MS Analysis

Six biological replicates in JEV- or mock-infected Neuro2a cells were set up for metabolomics detection. Extraction of metabolites and LC-MS/MS analysis were provided by Biotree Biotech (Shanghai, China).

The metabolites with the variable importance in the projection (VIP) > 1 and P-value of Student's t-test < 0.05 were considered as significantly changed. In pattern-specific analysis such as glucose metabolism, purine and pyrimidine metabolism and lipid metabolism, metabolites in positive ion mode (POS) and negative ion mode (NEG) were analyzed together. When a metabolite was detected both in POS and NEG, the one with higher MS2 score was picked.

RNA Extraction and Transcriptome Sequencing

Three biological replicates in JEV- or mock-infected Neuro2a were set up. Total RNA extraction, transcriptome sequencing and differential expression analysis were provided by Biotree Biotech (Shanghai, China). Genes with |Fold Change| ≥ 1.5 and adjusted P-value < 0.05 were assigned as differentially expressed.

Integrated Network Analysis of Transcriptomics and Metabolomics

The P-value and fold change of both differential expressed genes and metabolites were collated and summarized for network analysis. The metabolite-transcript regulatory networks were visualized using Cytoscape v3.6.1 software (San Diego, CA, USA).

Assay for Lactate

Lactate in Neuro2a cells infected with Mock and JEV at 24 hpi and 48 hpi was determined by Lactic Acid assay kit (Nanjing Jiancheng Bioengineering Institute, China) according to the manufacturer's instructions.

Flux Analyses

Cellular oxygen consumption rate (OCR) was measured using Seahorse XF-24 Metabolic Flux analyzer (Seahorse biosciences, Agilent). 1×10^5 Neuro2a cells were seeded in XF24 24-well plate until adherent and then infected with mock or JEV for 24 h. Basal respiration was measured in the absence of 2 mmol/L pyruvate and 25 mmol/L glucose. After the assessment of OCR in basal condition, 1 μmol/L oligomycin, 0.75 μmol/L carbonylcyanide p-triflouromethoxyphenylhydrazone (FCCP) and 1 μmol/L rotenone were subsequentially added. All OCR values were normalized to cell number after the experiment. All results were averages of five biological replicates.

Real-time RT-qPCR

Total RNA from cells was extracted with Total RNA Kit I (Omega, USA) and used as the template for reverse transcription. cDNA was synthesized using Hifair® II 1st Strand cDNA Synthesis Kit (Yeasen, Shanghai, China). qRT-PCR experiments were carried out using Hieff® qPCR SYBR Green Master Mix (Yeasen, Shanghai, China) according to the manufacturer's instructions to measure transcripts or JEV RNA levels. The level of mRNA expression was normalized with *β-actin*. The sequences of primers are listed as supplementary information (Supplementary Table S1).

Western Blot Analysis

Cells were lysed with RIPA Lysis and Extraction Buffer (ThermoFisher, USA) containing PMSF (ThermoFisher, USA) protease inhibitor. The titer of total protein was quantified using Protein Reagent Assay BCA Kit (ThermoFisher, USA). Western blot analysis was carried out according to the standard method. Antibodies used in this research were as follows: rabbit anti-JEV NS3 (GeneTex, CA) at 1:3000, rabbit anti-HK2 (Proteintech, China) at 1:2000, rabbit anti-OGDH (Proteintech, China) at 1:2000, rabbit anti-β-tubulin (Proteintech, China) at 1:8000. The PVDF membranes were visualized by infrared imaging system (Odyssey, LI-COR, USA).

Plaque-Forming Assay

BHK-21 cells (2×10^5/well) were seeded into 12-well culture plates and incubated overnight. Supernatants of cells were removed and then, cells were washed twice with PBS. Serial tenfold diluted samples collected from Neuro2a or primary neurons were added and incubated at 37 °C for 2 h. After viral adsorption, cell monolayer was covered with overlay medium (25 mL 4 × DMEM, 25 mL ddH_2O, 50 mL 4% methycellulose and 2 mL FBS) for 5 days. Then, the overlay medium was removed and cell monolayer was stained with 1% crystal violet.

Statistical Analysis

Except for special statistical analysis of transcriptome and metabolome described above, other statistical analyses used GraphPad Prism version 8.1 (GraphPad, CA). Statistical comparation were made by Student's t-test.

P-values < 0.05 were considered significant ($*P < 0.05$, $**P < 0.01$, and $***P < 0.001$).

Results

Differential Metabolite Identification and Pathway Enrichment Analysis

Since the level of JEV genome in Neuro2a cells at different time-points post of infection had been detected, the time point of 24 h (defined as the early stage of infection compared to 48 h in our research) was seen as the high-efficiency replicative period and more favorable for the study of cellular metabolomics reprogramming induced by JEV infection (Supplementary Fig. S1). Multivariate pattern recognition analyses were conducted after original metabolomics data management to provide an overview of the metabolomic changes. Principle component analysis (PCA, Supplementary Fig. S2A, S2B), supervised orthogonal projections to latent structures-discriminant analysis (OPLS-DA, Supplementary Fig. S2C, S2D) and permutation test of OPLS-DA models (Supplementary Fig. S2E, S2F) were applied and suggested the distribution between JEV-infected group and mock-infected group was notably distinguished.

Differential metabolites were determined by the combination of the VIP value (> 1) in OPLS-DA model and the *P*-value (< 0.05) from student's *t*-tests. A total of 69 differential metabolites in NEG and 58 in POS were identified by mass spectrum matching (MS2 matching in human metabolome database and Kyoto Encyclopedia of Genes and Genomes (KEGG) database). Compared to the mock-infected group, 25 metabolites were significantly up-regulated and 44 metabolites down-regulated in NEG, and 24 metabolites were up-regulated and 34 metabolites were down-regulated respectively in POS. A volcano plot was performed for visualizing all differential metabolites detected between JEV and mock-infected Neuro2a cells (Fig. 1A, 1B).

To explore the potential metabolic pathways affected by JEV infection, differential metabolites were annotated and assigned based on KEGG database (http://www.kegg.jp/kegg/pathway.html). The enrichment analysis of KEGG pathways included 16 pathways in NEG and 8 pathways in POS, specifically containing energy metabolism, material transportation, signal transduction, cell cycle regulation and other cellular physiological and biochemical processes. The KEGG enrichment treemap both in NEG (Fig. 1C) and POS (Fig. 1D) visualized all enriched pathways based on the number of enriched differential metabolites and *P*-value. Taking the treemap in NEG as an example, JEV infection mainly affects glutathione metabolism, vitamin B6 metabolism, glycerolipid metabolism and pyrimidine metabolism. Glutathione always plays a key role in the maintenance of cellular redox homeostasis. The decreased level of glutathione [fold change (FC) (JEV vs. mock) = 0.72], may be closely associated with neuron damage caused by oxidative stress during encephalitis. Pathways related to lipid metabolism, like glycerolipid metabolism in NEG, sphingolipid metabolism (sphingosine, FC = 0.53) and glycerophospholipid metabolism (choline, FC = 2.07) in POS, were also significantly enriched in KEGG pathway analysis. These results revealed that lipid metabolism was markedly modulated in JEV infected neuron cells and coincided with the findings of other flaviviruses like ZIKV and DENV (Martin-Acebes *et al.* 2016). The involvement of lipids in flavivirus biology can be from virion attachment, intracellular membrane remodeling, viral particle assembly interact with lipid droplet, to the regulation of cellular autophagy and apoptosis (Leier *et al.* 2018). Nucleotides as the basic materials both for cell proliferation and viral genome replication, were also obviously reprogrammed during JEV infection as evidenced by enriched purine and pyrimidine metabolism in NEG and POS displayed in Fig. 1.

Taken together, the metabolic reprogramming induced by JEV infection is reflected in a variety of biological functional pathways.

Transcriptome Analysis of JEV Infected Neuro2a Cells

Genes with fragments per kilobase million (FPKM) value greater than 1 in the transcriptomics data were considered as expressed genes. Venn diagram (Fig. 2A) demonstrated the distribution of the number of genes annotated only in JEV-infected (568), mock-infected (547), or in both groups (11,832). Transcriptional changes in response to JEV infection were determined and the screening conditions for differentially expressed genes (DEGs) were $|\text{Fold-Change}| \geq 1.5$ and Padj (a common form of false discovery rate) < 0.05. A total of 4709 DEGs were identified based on the stringent statistical threshold, of which 2343 were up-regulated and 2366 were down-regulated (Fig. 2B). The top 20 most significantly enriched KEGG pathways both in up-regulated and down-regulated mode were selected to produce the scatter plot (Fig. 2C, 2D).

DEGs up-regulated in JEV-infected Neuro2a cells were mainly linked to pathways representing inflammatory processes including IL-17 signaling pathway, NF-kappa B signaling pathway, and TNF signaling pathway. The majority of down-regulated DEGs were involved in pathways associated with metabolism, especially the metabolism of lipid species. Biosynthesis of unsaturated fatty acids, sphingolipid metabolism, steroid biosynthesis and

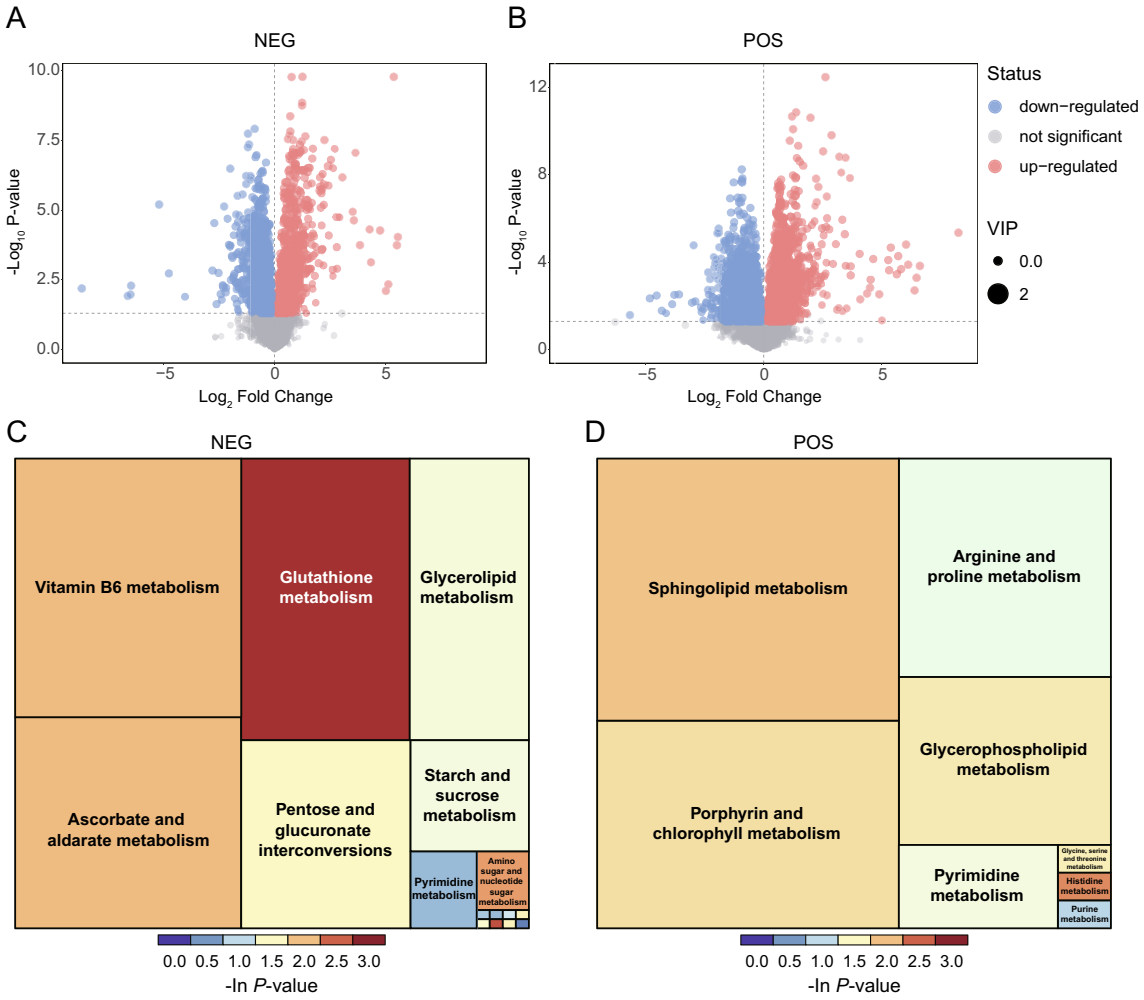

Fig. 1 Differential metabolite identification and pathway enrichment analysis. Volcano plot for JEV- vs mock group in negative ion mode (NEG) (**A**) and positive ion mode (POS) (**B**). Each plot represents a metabolite identified. Significantly up-regulated metabolites were labeled as red points, while the down-regulated metabolites were marked as blue points. Treemap plot of pathway enrichment based on KEGG pathway analysis for JEV-infected group vs mock group in NEG (**C**) and POS (**D**). The area size of the square indicates the impact of the pathway in the topology analysis, and the color represents the *P* value of the enrichment analysis [take the negative natural logarithm, -ln(p)].

fatty acid metabolism were markedly down-regulated, which is somewhat different from other flaviviruses infection processes, where the lipid biosynthesis were mostly enhanced (Zhang *et al.* 2019b). This phenomenon indicated that JEV was more likely to prefer consuming lipid components within host cells, rather than promoting lipids biosynthesis to maintain virus proliferation in the early infection stage.

Glycolysis Is Essential for Optimal Replication of JEV

Through the specific-pattern analysis of metabolomics, we found that metabolites in the glycolysis pathway, such as pyruvate and lactate were all not significantly changed at 24 hpi (Fig. 3A). Duplicate test of cellular lactate was performed at 24 and 48 hpi subsequently for further validation. As shown in Fig. 3B, lactate contents were significantly increased with the increase of JEV infection time, which indirectly reflected enhanced glycolytic activity in JEV-infected Neuro2a cells. Thus, the content of pyruvate and lactate were not significantly changed in the early infection stage (24 hpi) may be due to their participation in the biosynthesis of multiple metabolites. Meanwhile, the level of malate, a metabolite near the end of the tricarboxylic acid (TCA) cycle, showed a statistically significant decreasing trend (FC = 0.70, $P < 0.05$).

In addition, genes both involved in glycolysis and TCA cycle were analyzed and represented as a heatmap (Fig. 3C). The protein level of representative rate-limiting enzymes in the glycolysis pathway and TCA cycle were also detected in Neuro2a cells at 24 hpi (Fig. 3D). The

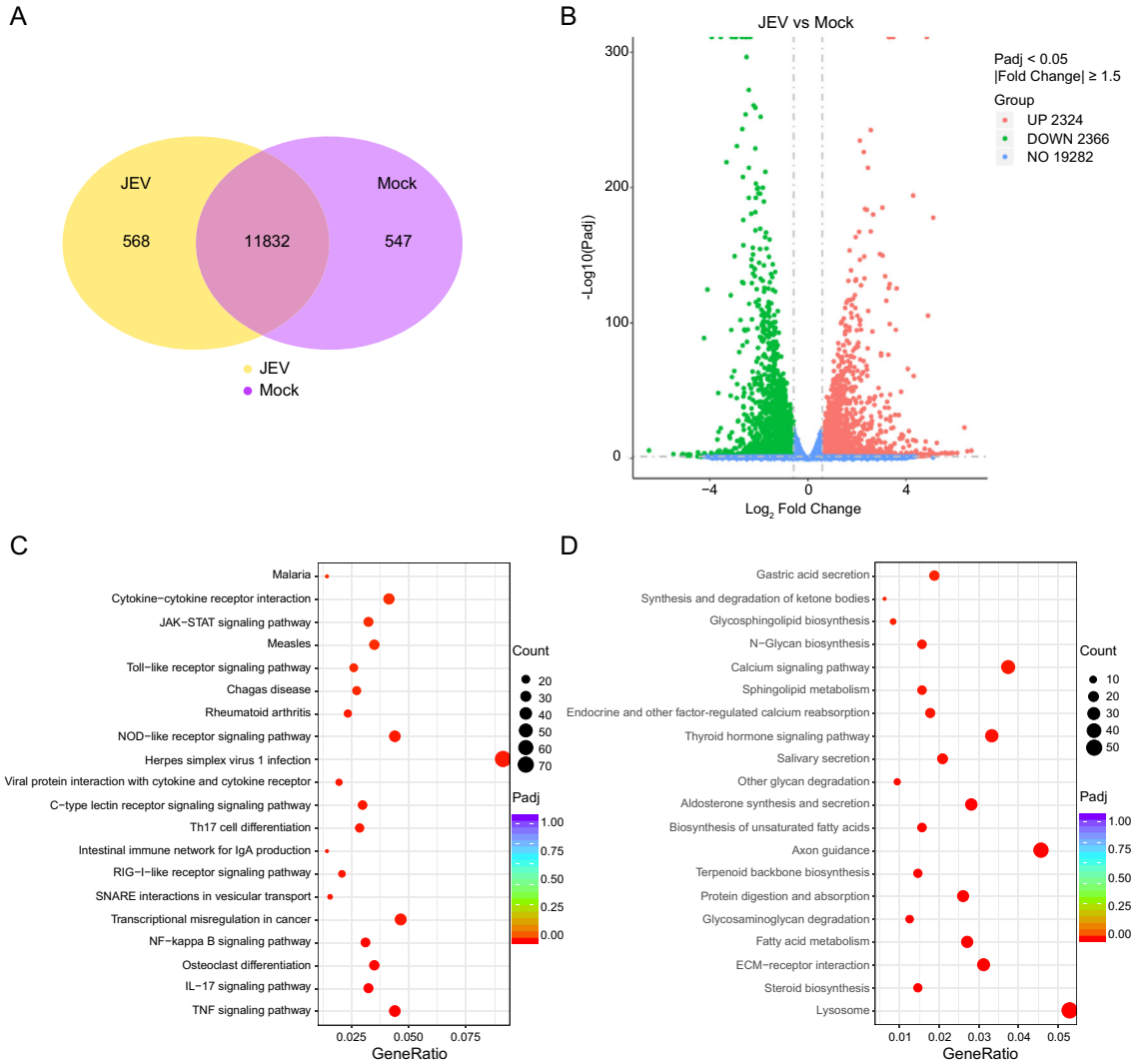

Fig. 2 Transcriptome analysis in JEV and mock-infected Neuro2a cell line. **A** Venn diagram of differential expressed genes between JEV and mock group. **B** Volcano plot analysis using $\log_2$(fold change) as X-axis and $-\log_{10}$(Padj) as Y-axis. The up-regulated genes presented in red, whereas the down-regulated genes in green. Genes without significant statistic difference are presented in blue. The gray line shows the statistical significance cutoff used in this study. **C**–**D** KEGG pathway enrichment analysis. Up-regulated pathways were shown in (**C**), and down-regulated in (**D**). (Ordinate: the KEGG signal path; abscissa: gene ratio). Gene ratio is the ratio of the differentially expressed gene number in certain pathway to the total gene number in this pathway. The size of the dots represents gene ratio and the color of the dots represents enrichment significance

expression level of hexokinase 2 (HK2), the first rate-limiting enzyme in the glycolysis pathway, was increased in JEV-infected Neuro2a cells. However, there is an inconsistency of HK2 mRNA level with protein level. We speculated that this inconsistency, on the one hand, might be due to the negative feedback of cumulative protein on its mRNA level, and on the other hand, due to the different degradation rate between protein and mRNA (Muller-McNicoll *et al.* 2019).

Meanwhile, the level of 2-oxoglutarate dehydrogenase (OGDH), a key enzyme in TCA cycle, was down-regulated. These results suggested that increased glycolysis and decreased OXPHOS in Neuro2a cells occurred during JEV infection. Then, oxygen consumption rate (OCR) was detected both in JEV- or mock-infected Neuro2a cells confirmed the impairment of OXPHOS under JEV infected condition (Fig. 3E).

Since glycolysis flux apparently increased during JEV infection, we employed 2-DG, a competitive inhibitor targeting hexokinase, to block glycolysis activity. Cell viability assay was performed in Neuro2a cell line treated with various concentrations of 2-DG and showed a non-cytotoxic effect (Supplementary Fig. S3A). The results showed that 2-DG could effectively inhibit JEV replication both in Neuro2a cell line (Fig. 3F, 3G) and mouse primary neurons (Fig. 3H). Furthermore, the addition of 2-DG at

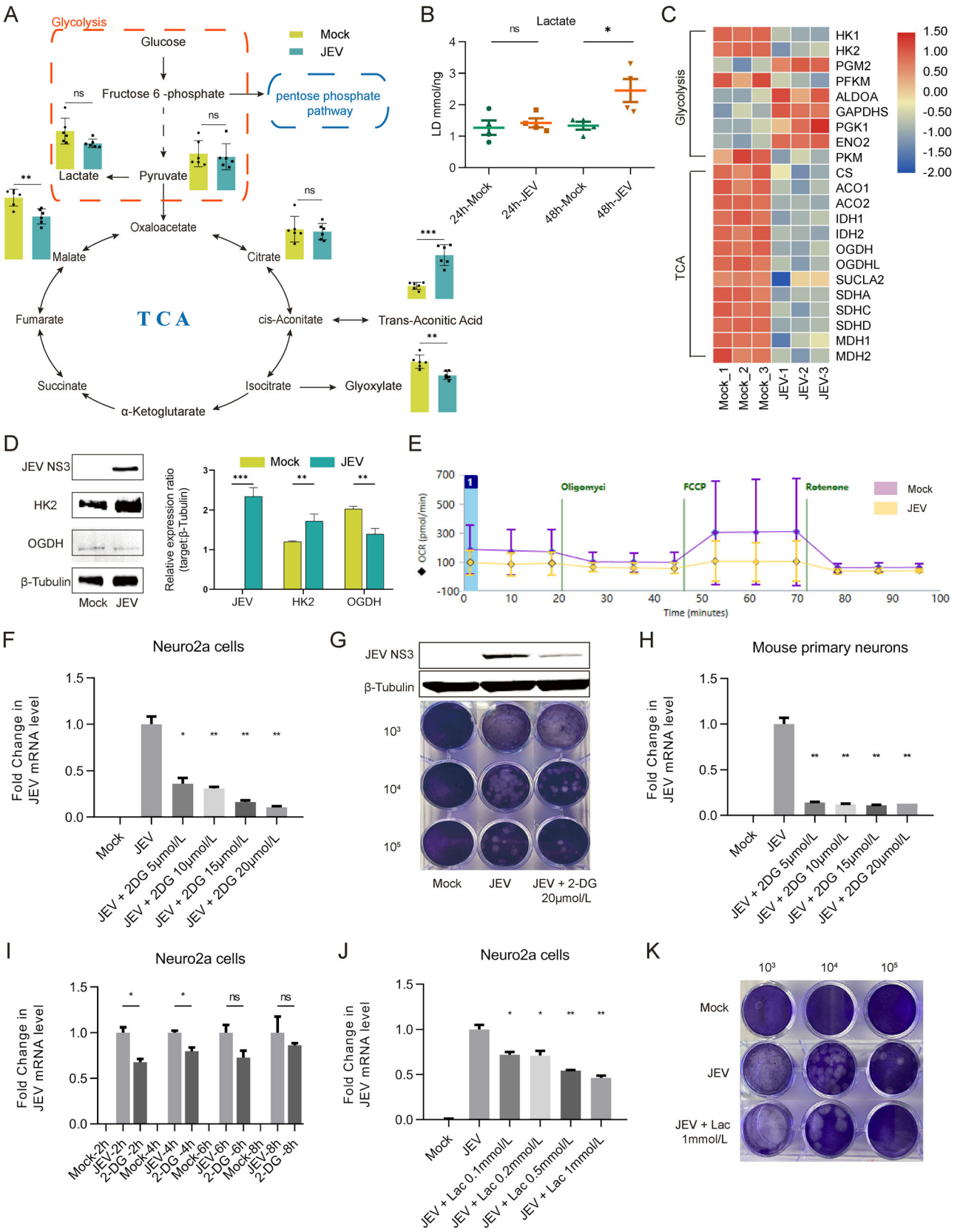
A
Glycolysis
Glucose
Mock
JEV
Fructose 6 -phosphate
pentose phosphate pathway
Lactate
Pyruvate
Oxaloacetate
Malate
Citrate
Fumarate
T C A
cis-Aconitate
Trans-Aconitic Acid
Succinate
Isocitrate
Glyoxylate
α-Ketoglutarate
B
Lactate
LD mmol/ng
24h-Mock
24h-JEV
48h-Mock
48h-JEV
C
Glycolysis
TCA
HK1
HK2
PGM2
PFKM
ALDOA
GAPDHS
PGK1
ENO2
PKM
CS
ACO1
ACO2
IDH1
IDH2
OGDH
OGDHL
SUCLA2
SDHA
SDHC
SDHD
MDH1
MDH2
Mock_1
Mock_2
Mock_3
JEV-1
JEV-2
JEV-3
D
JEV NS3
HK2
OGDH
β-Tubulin
Mock JEV
Relative expression ratio (target:β-Tubulin)
JEV
HK2
OGDH
E
OCR (pmol/min)
Oligomyci
FCCP
Rotenone
Mock
JEV
Time (minutes)
F
Neuro2a cells
Fold Change in JEV mRNA level
Mock
JEV
JEV + 2DG 5μmol/L
JEV + 2DG 10μmol/L
JEV + 2DG 15μmol/L
JEV + 2DG 20μmol/L
G
JEV NS3
β-Tubulin
Mock
JEV
JEV + 2-DG 20μmol/L
H
Mouse primary neurons
Fold Change in JEV mRNA level
I
Neuro2a cells
Fold Change in JEV mRNA level
J
Neuro2a cells
Fold Change in JEV mRNA level
JEV + Lac 0.1mmol/L
JEV + Lac 0.2mmol/L
JEV + Lac 0.5mmol/L
JEV + Lac 1mmol/L
K
Mock
JEV
JEV + Lac 1mmol/L

◀**Fig. 3** Glycolysis is essential for optimal replication of JEV. **A** Intermediates of glucose metabolism detected in Mock and JEV infected Neuro2a cells. **B** Lactate levels in Neuro2a cells were detected at 24 hpi and 48 hpi. **C** Heatmap analysis of expression levels of genes involved in glycolysis and TCA cycle. **D** Detection of JEV NS3, HK2 and OGDH proteins in Neuro2a cells infected with mock and JEV at 24 hpi. **E** Oxygen consumption rate (OCR) was detected both in JEV or Mock infected Neuro2a cells by Seahorse extracellular fluxanalyzer. **F** JEV mRNA levels in mock and JEV-infected Neuro2a cells treated with 2-DG at 24 hpi. **G** Detection of JEV NS3 protein level and infectious viral particles released in cell culture medium. **H** Viral mRNA levels in mock and JEV-infected mouse primary neurons treated with 2-DG at 24 hpi. The level of mRNA expression was normalized with *β-actin*. **I** Addition of 2-DG at various time-points post infection showed an important role of glycolysis in supporting the early steps of viral infection. **J** Viral mRNA levels in mock and JEV-infected Neuro2a cells treated with lactate at 24 hpi. **K** Exogenous addition of lactate could inhibit JEV replication in Neuro2a cells. 10^3, 10^4 and 10^5 represented the dilution rate. *, $P < 0.05$; **, $P < 0.01$; ***, $P < 0.001$; ns, not significant.

various time-points post of infection showed that the inhibitory effect of 2-DG on JEV replication could only exert at the early stage of the viral life cycle (2 hpi and 4 hpi) and showed an important role of glycolysis in the early steps of viral infection (Fig. 3I). This result is consistent with norovirus infection in RAW cells (Passalacqua *et al.* 2019).

Since the content of lactate gradually accumulated with infection, we further evaluated its effect on JEV replication. Of note, addition of lactate into Neuro2a cells infected with JEV could effectively inhibit JEV replication (Fig. 3J, 3K). The possible reason might be that increased lactate provided negative feedback inhibition of glucose utilization and glycolysis activity (Brooks 2020). Taken together, these results demonstrated that glycolysis is essential for optimal JEV propagation.

PPP is Indispensable for JEV Replication

Universally, PPP is a major branch pathway of glycolysis for *de novo* nucleotide synthesis. Although metabolites in this pathway had not changed significantly, the levels of some substances in downstream, such as metabolites associated with purine and pyrimidine metabolism were pronounced affected by JEV infection (Fig. 4A). Except for some metabolites in the early steps of purine synthesis such as AICAR, dIMP and D-ribose-1P, the level of other metabolites was mainly reduced upon JEV infection, mostly owing to the heavily reliance on host nucleotide intermediates for viral genome production. Since nucleotide metabolism plays a crucial role in viral replication, PPP inhibitor 6-Aminonicotinamide (6-AN) was applied to determine the effect of PPP on JEV infection. It is clear that PPP is of great importance in maintaining cellular physiological proliferation, its blocking will inevitably affect the cell's own replication process (Supplementary Fig. S3B). However, the inhibitory effect of 6-AN on JEV propagation is extremely obvious at the viral genome, protein expression and released infectious viral particles level both in Neuro2a cell line (Fig. 4B–4D) and mouse primary neurons (Fig. 4E–4G). On the one hand, this may be partly owing to the negative effect of 6-AN on cellular proliferation, and on the other hand, perhaps due to the inhibitory effect of 6-AN on nucleotides synthesis, which reduces nucleotide precursors required for viral genome replication. Furthermore, we supplemented D-ribose-5-phosphate, the final product of PPP and generally be used in the synthesis of nucleotides, under 6-AN treatment condition (Fig. 4H). The results showed that anaplerosis of D-ribose-5-phosphate could partially restore the replication of JEV and suggested the indispensable role of PPP in providing nucleotide precursors in JEV-infected neurons.

JEV Rewires Cellular Lipid Metabolism

To further clarify the changes in the metabolic profile of Neuro2a cells during JEV infection, the metabolic-transcriptomic regulatory network was constructed based on the integrated analysis of DEGs and differential metabolites identified in POS (Fig. 5A). (Since network analysis of NEG was similar to POS, the results were not exhibited here). The systematic network showed a complex correlation between metabolites and DEGs and, it is to be noted that lipid metabolism (red dotted box in Fig. 5A) was highly aggregated in the overall network analysis. It indicated that the anabolism and catabolism of lipid species were thoroughly reprogrammed in neurons during JEV infection. Network of Lipid-associated metabolites and DEGs were further performed and indicated that lipid metabolism might be the key biological process related to virus propagation and the development of encephalitis (Supplementary Fig. S4).

Then, metabolites related to lipid metabolism were filtered and visualized as a heatmap to reveal the cellular lipid metabolism profile (Fig. 5B). Most of them displayed a downward trend after JEV infection, suggesting a heavy consumption of lipids to maintain virus replication. Meanwhile, genes which encode rate-limiting enzymes in fatty acid biosynthesis, such as fatty acid synthase (FASN, FC = −1.59) was also down-regulated at 24 hpi in transcriptomics data. This suggests that lipid species were mainly consumed by catabolism at the early stage of JEV infection.

It is noteworthy that metabolites within arachidonic acid metabolism, such as 20-hydroxyeicosatetraenoate (20-HETE, FC = 1.44) and prostaglandin D2 (PGD2, FC = 2.12) were significantly up-regulated in JEV-infected

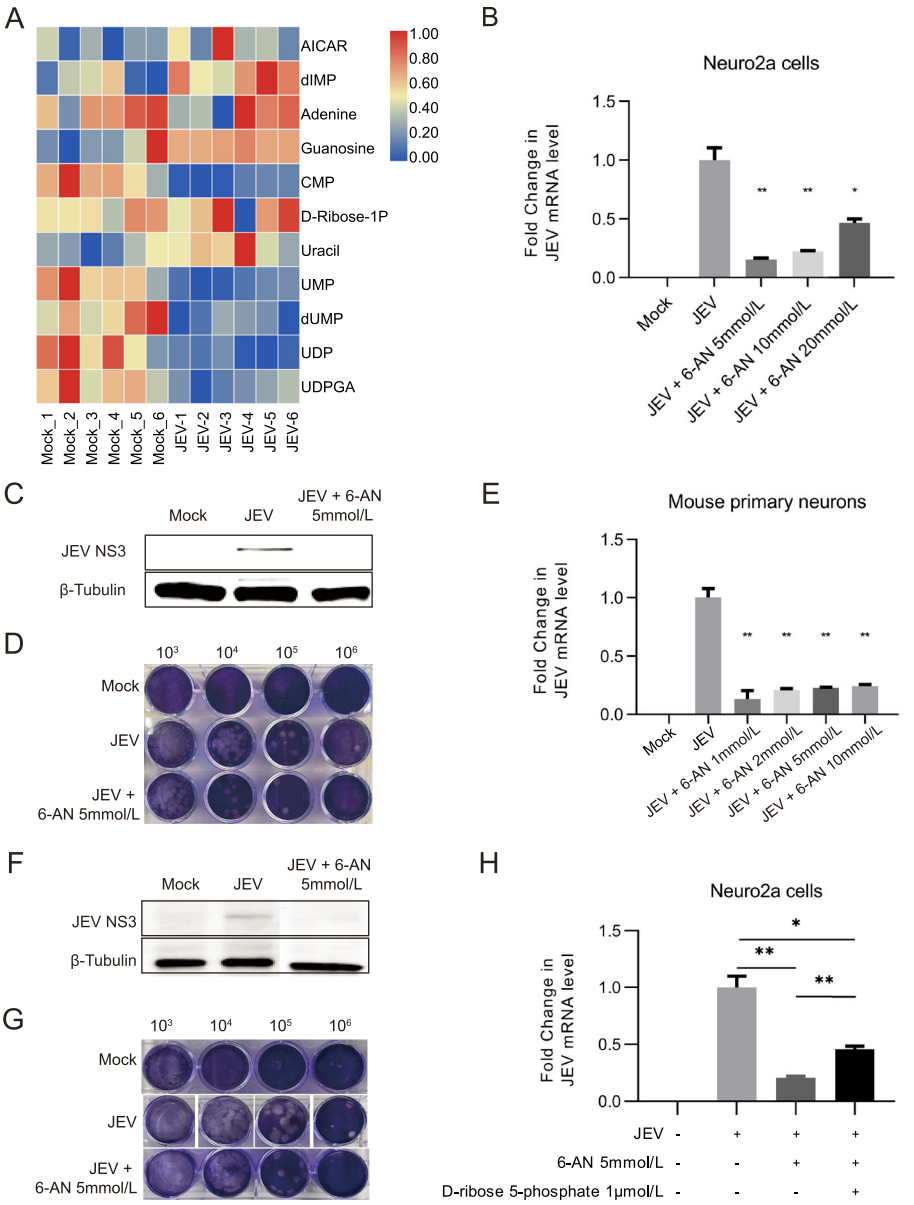

Fig. 4 PPP is indispensable for JEV replication. **A** Heatmap analysis of significantly changed metabolites associated with purine and pyrimidine metabolism. **B–G** Intervention of PPP by 6-AN significantly inhibits JEV replication in Neuro2a cell line and mouse primary neurons at 24 hpi. JEV mRNA levels in JEV-infected Neuro2a cells (**B**) and mouse primary neurons (**E**) treated with 6-AN at 24 hpi were detected by qPCR analysis. The level of mRNA expression was normalized with *β-actin*. The expression levels of viral protein NS3 in JEV-infected Neuro2a cells (**C**) and mouse primary neurons (**F**) were detected by Western blot analysis. Plaque formation assay shows the reduction of plaque generation in JEV-infected Neuro2a cells (**D**) and mouse primary neurons (**G**). 10^3, 10^4, 10^5 and 10^6 represented the dilution rate. **H** qPCR analysis of JEV mRNA level shows that anaplerosis of D-ribose 5-phosphate under 6-AN treatment condition could partially restore the viral replication. *, $P < 0.05$; **, $P < 0.01$.

Neuro2a cells. Metabolites related to arachidonic acid metabolism generally served as pro-inflammatory mediators in promoting cellular oxidative stress. Thus, the increased level of 20-HETE and PGD2 might be partially responsible for the progression of encephalitis.

The level platelet-activating factor (PAF), which is involved in the increase of vascular permeability and the infiltration of leukocytes, was also markedly increased in JEV-infected Neuro2a cells. Previous studies on the model of herpes simplex virus type-1 (HSV-1) encephalitis have confirmed that PAF is closely involved in leukocytes infiltration and disease progression (Brooks 2020). The increased content level of PAF (FC = 2.35) in our metabolomics data might also play a similar role in encephalitis caused by JEV infection.

We next investigated whether lipid metabolism is required for optimal JEV infection by intervening host cell lipid metabolic process through several inhibitors (Fig. 5C). ND-630, an inhibitor of acetyl-CoA carboxylase (ACC) dimerization, was used to repress fatty acid synthesis and showed a potent antiviral effect in Neuro2a cells (cell viability assay seen in Supplementary Fig. S3C). Furthermore, interfering fatty acid beta-oxidation with carnitine palmitoyltransferase-I (CPT-1) inhibitor Etomoxir also exhibited an inhibitory effect on JEV replication (Cell viability assay seen in Supplementary Fig. S3D). Since lipid species were mainly catabolized within 24 h of JEV infection, lipolysis inhibitor ATGL was used to clarify the effect of lipolysis on JEV replication (No cytotoxicity when the concentration under 50 μmol/L (Mayer *et al.*

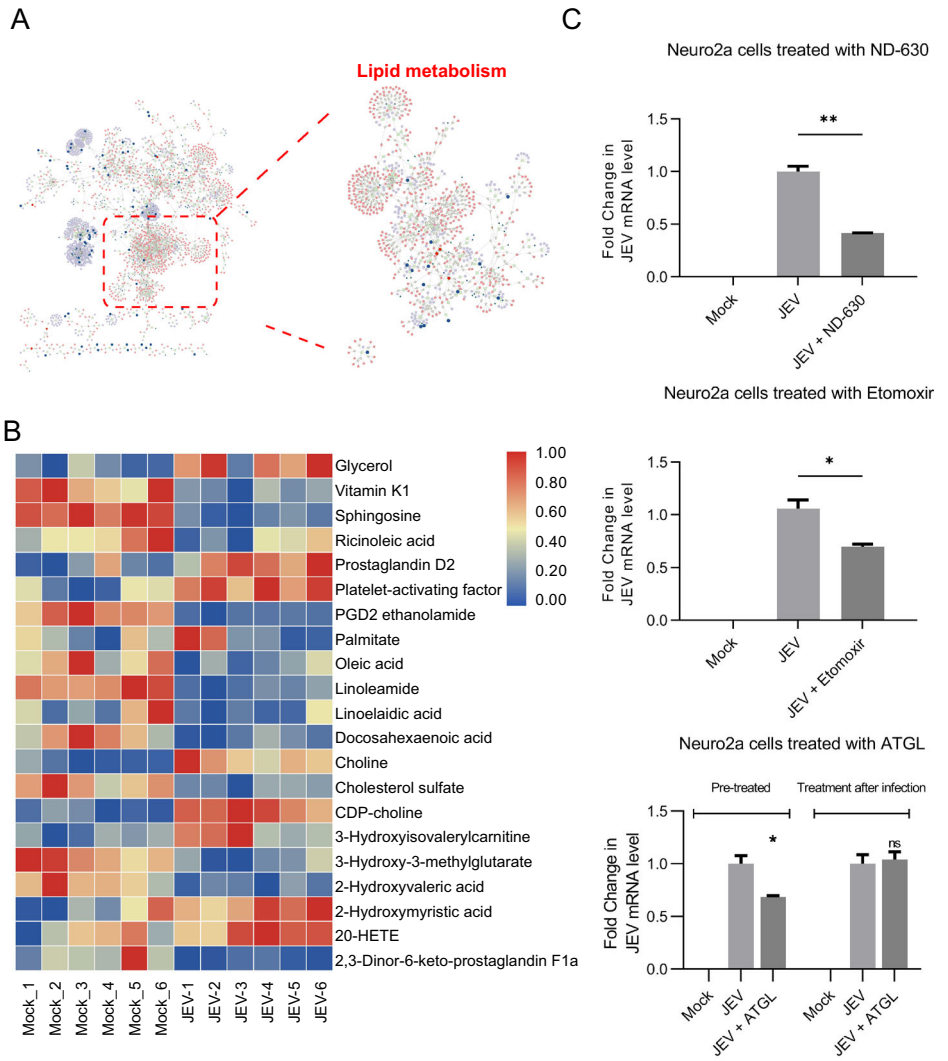

Fig. 5 Reprogramming of lipid metabolism in neuro2a during JEV infection. **A** Integrated network analysis of metabolomic and transcriptomic profiling reveals lipid metabolism was significantly reshaped during JEV infection. **B** Heatmap showing relative levels of the lipids, sterols, and their derivatives. **C** The effect of lipid metabolism related inhibitors on JEV replication. JEV mRNA levels were detected by qPCR analysis. The level of mRNA expression was normalized with *β-actin*. ND-630: 0.5 nmol/L; Extomoxir: 0.5 μmol/L; ATGL: 0.5 μmol/L. $*P < 0.05$; $**P < 0.01$; ns, not significant.

2013). It suggested that pretreatment of Neuro2a with ATGL for 12 h would significantly impede virus replication, while treatment after infection had no obvious effect.

Discussion

It is no wonder that viruses rely on host cell machinery to complete their entire life cycle. Intracellular metabolic status is an intrinsic factor that determines the successful viral infection and replication. Different viruses adopt diverse strategies to exploit host metabolism to optimize their replication (Thaker *et al.* 2019b; Thyrsted and Holm 2020). Currently, advanced techniques have been widely applied to reveal comprehensive interactions between virus and host in cellular metabolic facet, and then, explore potential antiviral tactics targeting virus-inducing metabolic re-programming.

Metabolomic approach is a common method for metabolic profile depicting in viral infection field. Central carbon metabolism comprised by glycolysis, PPP, and TCA cycle is predominant in maintaining a variety of cellular physiological functions and certainly vulnerable to be reprogrammed during viral infection. Metabolomic analyses of most DNA viruses, such as human cytomegalovirus (HCMV) (Rodriguez-Sanchez and Munger, 2019), Epstein-Barr virus (EBV) (Cai *et al.* 2017), and Kaposi's sarcoma-associated herpesvirus (KSHV) (Ma *et al.* 2015), suggest that central carbon metabolism has been reshaped by more similar approaches. The main manifestations are increased glucose uptake and glycolysis flux. In contrast to DNA viruses, metabolic manipulation strategies of RNA viruses are generally diverse (Mayer *et al.* 2019).

Take flaviviruses as examples, the global intracellular metabolic profiles of human foreskin fibroblasts suggest that central carbon metabolism, especially glycolytic pathway in glucose utilization, was significantly perturbed

during DENV infection (Fontaine *et al.* 2015). Viral non-structural protein NS1 could directly interact with glycolytic enzyme gluceralde-hyde-3-phosphate dehydrogenase (GAPDH) and lead to increased glycolytic flux (Allonso *et al.* 2015). However, the infection of ZIKV exhibits distinct effects on glucose metabolism in human versus mosquito cells (Thaker *et al.* 2019a). The infection of ZIKV will promote increased glucose utilization both in the TCA cycle and amino acid generation within human cells. In contrast, viral infection of C6/36 mosquito cells promotes glucose utilization via glycolysis and PPP, but decreases its contribution to the TCA cycle. Thus, dissimilar cellular outcomes with the cell death observed in ZIKV-infected human cells and survival observed in ZIKV-infected mosquito cells were caused. Different viruses usually have distinct metabolic requirements for their replication, and therefore exhaustive investigations are needed to reveal the metabolic interaction between certain pathogens and host cells.

Our study takes advantage of the integration of metabolomic and transcriptomic to unveil the global metabolic features in neuronal cells during JEV infection. Intermediates detected in central carbon metabolisms like lactate and malate suggested increased glucose contribution to glycolysis flux and decreased OXPHOS activity in JEV-infected Neuro2a cell line (Fig. 3A). Moreover, the expression levels of genes associated with glycolysis were also extremely different from TCA cycle, confirming the enhancement of glycolysis and the impairment of OXPHOS (Fig. 3B). It was consistent with the metabolic reprograming caused by most viruses previously reported. Host cells infected with viruses appear to display metabolic characteristics akin to the Warburg effect to satisfy the high bioenergetic and biosynthetic demands for virion production. One possible explanation is that increased flux of glycolysis and its branch PPP will be propitious to provide precursors for nucleotide synthesis and viral genome replication. In addition, lactate, the glycolytic product which plays an inhibitory role in cellular type I interferon response, will be accumulated with the enhancement of glycolysis (Zhang *et al.* 2019a). 2-DG and 6-AN were then employed to inhibit the glycolysis pathway and PPP. The results showed that both 2-DG and 6-AN could effectively inhibit JEV replication both in Neuro2a cell line and mouse primary neurons. These results indicated that glucose metabolism, both glycolysis and PPP are indispensable for the optimal propagation of JEV.

Lipidomic analyses of cells infected with flaviviruses have been well characterized over these years (Martin-Acebes *et al.* 2016, 2019). Conceptually, lipids are fatty acids and their derivatives, and substances biosynthetically or functionally related to these compounds (Fahy *et al.* 2011). Membrane-associated viral replication, particularly flaviviruses, is closely related to lipid synthesis, utilization, and transportation. It is generally known that the entry of flaviviruses depends on receptors located in lipid rafts for successful attachment. After internalization, the intracellular life cycle of flaviviruses is confined to the cytosol, thus remodeling cellular endomembranes into unique organelle-like structures, which are defined as viral replication compartments (VRCs), is crucial for virus genome replication (Miller and Krijnse-Locker 2008). These VRCs can not only increase the local concentration of cellular and viral factors that are required for sufficient genome replication, but shield genomic RNA from cellular innate immune sensors. Owing to its multivariable lipid profiles, the structures, membrane curvatures, and permeabilities of VRCs vary greatly between different flaviviruses (Strating and van Kuppeveld 2017). Glycerophospholipids (GLs), including phosphatidyl-inositol (PI), phosphatidyl-serine (PS), phosphatidyl-choline (PC) and phosphatidyl-ethanolamine (PE), are the most abundant and important structural lipids in the eukaryotic cellular membrane. Viruses generally remodel GLs metabolism to form a suitable membranous compartment for successful infection and replication by changing its ratio. The downstream product PI (FC = 1.95) in GLs synthesis was elevated in JEV infection, demonstrating the enhancement of GLs biosynthesis. Another component of cellular membranes, PS, was significantly down-regulated in JEV-infected Neuro2a cells (FC = 0.36). The biological reason might be that PS often acts as an “eat me” signal that promotes the engulfment of apoptotic cells (Chen *et al.* 2015). In this way, flaviviruses might take advantage of this PS-dependent uptake and infection termed as apoptotic mimicry mechanism (Mazzon and Mercer 2014). Therefore, mounts of PS might be used for the synthesis of mature viral envelope to mediate viral attachment and infusion. To be mentioned, the up-regulated of pro-inflammatory metabolites such as 20-HETE, PGD2 and PAF are particularly significant. These metabolites might be involved in the progression of encephalitis caused by JEV infection, thus partially inducing uncontrolled severe inflammation in brain (Hanna and Hafez 2018; Vilela *et al.* 2016).

Taken together, our study systematically described the metabolic landscape of neurons after JEV infection. Increased glycolysis flux and impaired OXPHOS in glucose utilization facilitate the biosynthesis of precursors needed for JEV replication. In addition, catabolic patterns of lipid metabolism were created to cope with the high anabolic demands of virion production and optimal virus propagation. Intervening host cell glucose metabolism and lipid metabolism by inhibitors showed potent antiviral effects and provided an auspicious therapeutic perspective on viral infectious diseases. This work provides further insights into the pathogenic mechanisms of JEV infection in the metabolic field and provides promising antiviral strategies by targeting metabolism.

Acknowledgements This research was funded by the National Major Science and Technology Projects of China, grant number 2017ZX10202203-007-003.

Author Contributions JL and YL designed the experiments. ML and JY carried out the experiments and wrote the original draft. CY, XY, HZ, CL and ZX analyzed the data. JL and YL reviewed the manuscript and provided the financial support. All authors read and approved the final manuscript.

Compliance with Ethics Guidelines

Conflict of interest The authors declare that they have no conflict of interest.

Animal and Human Rights Statement This article does not contain any studies with human or animal subjects performed by any of the authors.

References

Allonso D, Andrade IS, Conde JN, Coelho DR, Rocha DC, Da SM, Ventura GT, Silva EM, Mohana-Borges R (2015) Dengue virus NS1 protein modulates cellular energy metabolism by increasing glyceraldehyde-3-phosphate dehydrogenase activity. J Virol 89:11871–11883

Barrows NJ, Campos RK, Liao KC, Prasanth KR, Soto-Acosta R, Yeh SC, Schott-Lerner G, Pompon J, Sessions OM, Bradrick SS, Garcia-Blanco MA (2018) Biochemistry and molecular biology of flaviviruses. Chem Rev 118:4448–4482

Bian P, Zheng X, Wei L, Ye C, Fan H, Cai Y, Zhang Y, Zhang F, Jia Z, Lei Y (2017) MLKL Mediated necroptosis accelerates JEV-induced neuroinflammation in mice. Front Microbiol 8:303

Brooks GA (2020) Lactate as a fulcrum of metabolism. Redox Biol 35:101454

Cai TT, Ye SB, Liu YN, He J, Chen QY, Mai HQ, Zhang CX, Cui J, Zhang XS, Busson P, Zeng YX, Li J (2017) LMP1-mediated glycolysis induces myeloid-derived suppressor cell expansion in nasopharyngeal carcinoma. PLoS Pathog 13:e1006503

Chen YH, Du W, Hagemeijer MC, Takvorian PM, Pau C, Cali A, Brantner CA, Stempinski ES, Connelly PS, Ma HC, Jiang P, Wimmer E, Altan-Bonnet G, Altan-Bonnet N (2015) Phosphatidylserine vesicles enable efficient en bloc transmission of enteroviruses. Cell 160:619–630

Erlanger TE, Weiss S, Keiser J, Utzinger J, Wiedenmayer K (2009) Past, present, and future of Japanese encephalitis. Emerg Infect Dis 15:1–7

Fahy E, Cotter D, Sud M, Subramaniam S (2011) Lipid classification, structures and tools. Biochim Biophys Acta 1811:637–647

Fontaine KA, Sanchez EL, Camarda R, Lagunoff M (2015) Dengue virus induces and requires glycolysis for optimal replication. J Virol 89:2358–2366

Hanna VS, Hafez E (2018) Synopsis of arachidonic acid metabolism: a review. J Adv Res 11:23–32

Leier HC, Messer WB, Tafesse FG (2018) Lipids and pathogenic flaviviruses: an intimate union. PLoS Pathog 14:e1006952

Ma T, Patel H, Babapoor-Farrokhran S, Franklin R, Semenza GL, Sodhi A, Montaner S (2015) KSHV induces aerobic glycolysis and angiogenesis through HIF-1-dependent upregulation of pyruvate kinase 2 in Kaposi's sarcoma. Angiogenesis 18:477–488

Martin-Acebes MA, Jimenez DON, Saiz JC (2019) Lipid metabolism as a source of druggable targets for antiviral discovery against zika and other flaviviruses. Pharmaceuticals (basel) 12:97

Martin-Acebes MA, Vazquez-Calvo A, Saiz JC (2016) Lipids and flaviviruses, present and future perspectives for the control of dengue, Zika, and West Nile viruses. Prog Lipid Res 64:123–137

Mayer KA, Stockl J, Zlabinger GJ, Gualdoni GA (2019) Hijacking the supplies: metabolism as a novel facet of virus-host interaction. Front Immunol 10:1533

Mayer N, Schweiger M, Romauch M, Grabner GF, Eichmann TO, Fuchs E, Ivkovic J, Heier C, Mrak I, Lass A, Hofler G, Fledelius C, Zechner R, Zimmermann R, Breinbauer R (2013) Development of small-molecule inhibitors targeting adipose triglyceride lipase. Nat Chem Biol 9:785–787

Mazzon M, Mercer J (2014) Lipid interactions during virus entry and infection. Cell Microbiol 16:1493–1502

Miller S, Krijnse-Locker J (2008) Modification of intracellular membrane structures for virus replication. Nat Rev Microbiol 6:363–374

Muller-McNicoll M, Rossbach O, Hui J, Medenbach J (2019) Auto-regulatory feedback by RNA-binding proteins. J Mol Cell Biol 11:930–939

Passalacqua KD, Lu J, Goodfellow I, Kolawole AO, Arche JR, Maddox RJ, Carnahan KE, O'Riordan M, Wobus CE (2019) Glycolysis Is an Intrinsic Factor for Optimal Replication of a Norovirus. mBio 10:e02175–18

Rodriguez-Sanchez I, Munger J (2019) Meal for Two: Human Cytomegalovirus-Induced Activation of Cellular Metabolism. Viruses 11:273

Strating JR, van Kuppeveld FJ (2017) Viral rewiring of cellular lipid metabolism to create membranous replication compartments. Curr Opin Cell Biol 47:24–33

Su MA, Huang YT, Chen IT, Lee DY, Hsieh YC, Li CY, Ng TH, Liang SY, Lin SY, Huang SW, Chiang YA, Yu HT, Khoo KH, Chang GD, Lo CF, Wang HC (2014) An invertebrate warburg effect: a shrimp virus achieves successful replication by altering the host metabolome via the PI3K-Akt-mTOR pathway. PLoS Pathog 10:e1004196

Thaker SK, Chapa T, Garcia GJ, Gong D, Schmid EW, Arumugaswami V, Sun R, Christofk HR (2019a) Differential metabolic reprogramming by zika virus promotes cell death in human versus mosquito cells. Cell Metab 29:1206–1216

Thaker SK, Ch'Ng J, Christofk HR (2019b) Viral hijacking of cellular metabolism. BMC Biol 17:59

Thyrsted J, Holm CK (2020) Virus-induced metabolic reprogramming and innate sensing hereof by the infected host. Curr Opin Biotechnol 68:44–50

Vilela MC, Lima GK, Rodrigues DH, Lacerda-Queiroz N, Pedroso VS, de Miranda AS, Rachid MA, Kroon EG, Campos MA, Teixeira MM, Teixeira AL (2016) Platelet activating factor (PAF) receptor deletion or antagonism attenuates severe HSV-1 meningoencephalitis. J Neuroimmune Pharmacol 11:613–621

Warburg O (1956) On the origin of cancer cells. Science 123:309–314

Zhang W, Wang G, Xu ZG, Tu H, Hu F, Dai J, Chang Y, Chen Y, Lu Y, Zeng H, Cai Z, Han F, Xu C, Jin G, Sun L, Pan BS, Lai SW, Hsu CC, Xu J, Chen ZZ, Li HY, Seth P, Hu J, Zhang X, Li H, Lin HK (2019a) Lactate is a natural suppressor of RLR signaling by targeting MAVS. Cell 178:176–189

Zhang Z, He G, Filipowicz NA, Randall G, Belov GA, Kopek BG, Wang X (2019b) Host lipids in positive-strand RNA Virus genome replication. Front Microbiol 10:286